J Mater Sci (2008) 43:4962–4971
DOI 10.1007/s10853-008-2730-y

Orientation of silicon particles in a binary Al–Si alloy

C. D. Marioara · S. J. Andersen · A. Birkeland · R. Holmestad

Received: 11 October 2007 / Accepted: 16 May 2008 / Published online: 3 June 2008

Abstract The orientations Si-crystals take in aluminium, in an alloy with composition Al–1.3at%Si, were investigated by transmission electron microscopy. Hardness was measured for isothermal heat-treatments at 175 °C and 260 °C. Conditions analysed by TEM were 17 h at 175 °C and an additional 3 h at 260 °C, both containing a high density of small Si-crystals, the finest corresponding to 175 °C. Two main orientation relationships were found: (001)Al || (001)Si, [100]Al || [100]Si and (001)Al || (110)Si, [1 $\bar{1}$ $\bar{1}$]Si || [010]Al. The first accounted for approximately 60% of Si precipitates in condition 17 h_175 °C. Despite a high number density and well-aligned interfaces, the Si precipitates have negligible influence on hardness. Findings are consistent with Ge particles in Al–Ge alloys.

Introduction

Recent investigations of the age-hardening Al–Mg–Si (–Cu) alloys indicate that Si is important for nucleation of the precipitates [1, 2] and is also a key in understanding their atomic structures [3, 4]. Specifically, it has been found that all precipitate structures can be interpreted as different arrangements of Al, Mg, (Cu) atoms on a stacking of hexagonal planes of silicon with nearest in-plane Si–Si distances $\sim$4 Å. These planes are similar to the {111} planes of diamond silicon (with Si–Si distance 3.84 Å). They are stacked either in a ⟨010⟩Al direction with period 4.05 Å (of which more details are given below) or in a ⟨310⟩Al direction with period 6.74 Å [3]. The period 4.05 Å always exists in the precipitates, and defines the direction of their needle lengths.

Crystals of diamond Si are frequently observed in the Al–Mg–Si–(Cu) alloys [3, 4]. Many crystals have been found to have a ⟨110⟩ Si zone axis parallel to Al ⟨001⟩ in a way that the two ⟨111⟩ directions of the ⟨110⟩ Si zone coincide with ⟨010⟩Al and ⟨310⟩Al type directions, i.e. the according {111} planes are parallel with the before-mentioned hexagonal planes that exist in the precipitates. Using one specific choice of directions, the orientation relation of diamond Si-particles in the Al matrix can be written:

$$(110)\mathrm{Si} \,||\, (001)\mathrm{Al},\ [1\,\bar{1}\,\bar{1}]\ \mathrm{Si} \,||\, [010]\mathrm{Al},\ [1\,\bar{1}\,2]\ \mathrm{Si} \,||\, [100]\mathrm{Al}. \quad (1)$$

We find it more convenient to put the relation in terms of a rotation matrix which, when multiplied by a Si-vector, gives the corresponding direction in the Al-system:

$$R_{02} = \frac{1}{\sqrt{6}} \begin{pmatrix} 1 & -1 & 2 \\ \sqrt{2} & -\sqrt{2} & -\sqrt{2} \\ \sqrt{3} & \sqrt{3} & 0 \end{pmatrix} \quad (2)$$

This shows that the normal vectors of the two {111}Si planes in the [110] zone ([1$\bar{1}$ $\bar{1}$]Si and [1$\bar{1}$1]Si) are parallel with [010]Al and [$\frac{4}{\sqrt{2}}$ 10] Al. The latter is only 1.04° from [310]Al. Thus, [010]Al and [310]Al are normal vectors of two Si {111} planes of diamond silicon, and coincide with the normal vectors of the triangular {111}Si resembling planes that exist in the precipitates of the Al–Mg–Si–(Cu) system. All the precipitate phases in these systems are therefore related to the single orientation of the Si-particles as defined by Eqs. 1 and 2. Since the correspondence

C. D. Marioara (✉) · S. J. Andersen
SINTEF Materials and Chemistry, 7465 Trondheim, Norway
e-mail: calin.d.marioara@sintef.no

A. Birkeland · R. Holmestad
Department of Physics, Norwegian University of Science and Technology, 7491 Trondheim, Norway

between the hexagonal Si-network of the precipitates and {111} planes of Si is not obvious, and since it was the major reason for the current work, the network will be discussed in the following paragraph.

Si-crystals and the Si-network in precipitates of the Al–Mg–Si system

Figure 1 shows how unit cells of three structurally different precipitates in the Al–Mg–Si–(Cu) system, I (β'), II (U2), and III (B′/Q′/Q), may be superposed on the projection of a {111} Si plane [3, 4]. The super-cells in Fig. 1 may be compared with the projections of the real unit cells, and Si-positions fall close to the projected Si-positions in the real cells. The cell parameter of the (smaller) Si super-cell and real precipitate cell (parentheses) are given. The cell parameter in the viewing direction is equal to that of Al, i.e. 4.05 Å. The {111} planes in Si come in pairs, the two layers separated by 2.35 Å. In aluminium, (inside the precipitates) this double plane can be viewed as semi-occupied, which makes possible a lining up with the (010)Al planes (i.e. since separation is smaller here, 2.025 Å). The remaining atoms (Mg, Al, Cu, etc.) will use this network as a fundament, and fill in open spaces which will have a natural correspondence with the two remaining {111} pairs in Silicon. i.e. the atom positions of the precipitates projected along the hexagonal Si-grid (parallel with Al ⟨100⟩) correspond nearly with the ⟨111⟩ Si projection of the AA–BB–CC diamond stacking. It may be

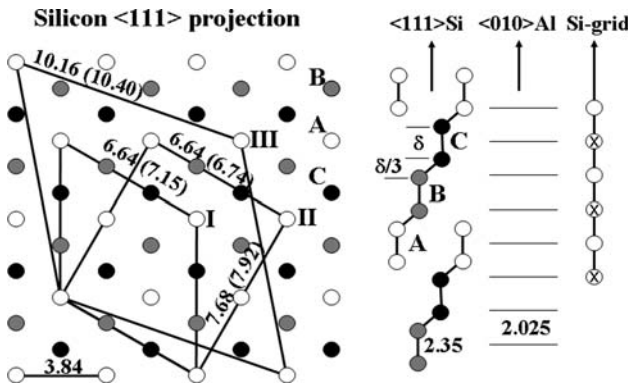

Fig. 1 Left: A ⟨111⟩Si diamond projection. All numbers are in angstrom (Å). White, grey, and black fill indicate the double layers A, B, C, also shown edge-on just to the right. This projection strongly resembles a hexagonal Si-grid found in all precipitates in Al–Mg–Si–(Cu) alloys. Super-cells of three common classes of precipitates are shown on the A-layer: I (β'), II (U2), III (B′ or Q′) [3, 4]. Real cell parameters are in parentheses. Precipitates grow as needles in the viewing direction. The grid is indicated on the far right side as a stacking of the semi-occupied AA-layers only ('x' means empty site of a Si-pair) parallel with {010} Al planes. Si-atoms of the precipitates project to A-positions, other atoms near B and C positions. The network has the same orientation as {111} planes of the Si-crystals of orientation O2, in the current work

noted that super-cells of most of the precipitates can also be found in aluminium. This means that the Si-grid and the aluminium matrix have rigid geometric relations. Thus, for most precipitates the Si-grid can be found to be locked in a specific direction with the matrix: two of the axes in the hexagon are near $\langle \bar{1}30 \rangle$ and $\langle 5\bar{1}0 \rangle$Al with angular separation 119.7°. As explained above, this corresponds with the orientation relationship as defined above in Eqs. 1 and 2. The strong correspondence between the precipitates and the Si-crystals indicates that the precipitates may nucleate/grow from small regions in the Al matrix where Si-atoms have arrangements closely related to the diamond structure. More information about this network and the precipitates may be found elsewhere [3, 4].

Al–Ge–(Si)–(Cu) alloys

Previous investigations by TEM on evolution of hardness, and shape and orientation of crystals in Al–Ge, Al–Ge–Si and Al–Ge–Si–Cu alloys (although heat-treatments and composition differ), are consistent with findings in this work [5–15]. A good overview of orientation and shape is given in [5]. A number of studies have demonstrated the importance of vacancies in nucleation, growth and shape of Al–Ge precipitates. For bibliography, confer [5, 15]. Some of these studies concern twinning and how it controls shape [5, 7, 8, 9]. They show that most orientation relations can be traced back to a few basic orientations via twinning. It is thus suggested that the orientation relations is influenced heavily by the vacancy concentration from the time of clustering [5, 7]. These two studies also go in depth concerning the shape of the crystals that was not the intention here. The size of the Ge atom is somewhat larger than silicon. This means that Ge should have an even stronger need for vacancies than Si, when forming clusters of some diamond character and using these clusters to form real particles with the diamond structure. Still nucleation and growth behaviour in the Al matrix seems to be similar. It appears, therefore, that the results from binary Al–Ge in most cases are transferable to the Al–Si system. We have presently unpublished results strongly indicating that Ge forms a similar hexagonal network in Al–Ge–Mg alloys, with precipitates isomorphous to the precipitates in the Al–Mg–Si–(Cu) system, which underlines the similarities further of Ge and Si. It may be noted also that in Al–Ge–Si alloys the early formed clusters [13] as well as precipitates contain both Ge and Si [14]. It is interesting also that in the Cu-containing alloys [9, 11, 12] the Si–Ge phase is heavily influencing nucleation of the Al–Cu phases (θ'',θ').

The major goal of this work has been to clarify what orientations Si-crystals take in a binary Al–Si alloy. In particular, it was checked if the same orientation relation as defined in Eqs. 1 and 2 would occur. The Si level was kept

at 1.3at%, which equals the level of solute (Mg + Si) in the Al–Mg–Si(–Cu) alloys analysed in previous studies [1, 4, 16].

Experimental

A pure Al–1.3at%Si alloy was homogenised for 2 h at 570 °C and extruded into the shape of thin bars having a rectangular cross-section 25 × 2 mm^2. The bars were cut into samples of dimensions 25 × 25 × 2 mm^3 and heat treated. The first set of specimens underwent solution treatment 1 h at 540 °C, water-quenching to room temperature (RT ∼ 25 °C), 4 h storage at RT and a final ageing at 175 °C between 30 min and 216 h. Samples for the second set initially were aged 17 h at 175 °C. From this temperature the specimens were water-quenched to RT followed by heat-treatments at 260 °C ranging from 10 min to 5 h. The specimens taken after different ageing times on the final heat-treatment stages were quenched in water. Vickers hardness measurements (1 kg load, 10 indentations per sample) were performed on these specimens using a Matsuzawa DVK—1S unit. The mean of 10 indentations per sample and corresponding standard error provided the data used to draw the hardness curves.

For the TEM investigations two heat-treatment conditions were selected, 17 h_175 °C and 3 h_260 °C, matching conditions used in previous studies of Al–Mg–Si(–Cu) alloys [1, 4, 16]. TEM specimens were prepared by electro-polishing in a Tenupol 3 machine. The electrolyte consisted of 1/3 HNO_3 in methanol where the solution was kept at temperatures between −20 °C and −35 °C. Conventional TEM analyses of the Si precipitates were performed using a Philips CM30T microscope operated at 150 kV, and for the high resolution (HR) work a JEOL 2010F microscope was used, operated at 200 kV. This instrument has a point resolution of approximately 2 Å. Due to the specific orientations Si precipitates take in respect to the Al matrix, all TEM investigations were performed with the matrix tilted in a ⟨100⟩Al zone axis, and all images shown in the present work are from this orientation.

Results

General microstructure, particles, homogeneity, hardness and strain

Bright field (BF) images like Fig. 2 reveal a large number of small Si- particles in the two analysed conditions. The particles have inhomogeneous distribution since significant volumes in the matrix are devoid of particles. In such depleted zones or in zones with lower numbers, precipitates are commonly coarser. TEM images show that precipitates in condition 17 h_175 °C are finer than in condition 3 h_260 °C. As is clear from Fig. 3, the hardness in both conditions is very low in spite of a high density of particles. In Fig. 3 the left curve (a) is the hardness response at 175 °C. The right curve (b) is the response at 260 °C, after an initial 17 h ageing at 175 °C. Similar hardness values have been obtained elsewhere [17] in an Al—1at% Si binary alloy. The low hardness is an indication that strain build-up along the interfaces of Si-particles with the Al matrix must be insignificant, although some small peaks in the 175 °C curve may indicate some temporary strain build-up until precipitates loose coherency. This was not investigated further. The hardness is three times higher after 17 h heat-treatment at 175 °C in Al–Mg–Si alloys, where between 30% and 60% of Si is substituted by Mg [1, 4, 16].

Shape and coherency relations of the Si-particles

The Si-particles can have pyramidal shape, be plates or rectangloids, or take a more equi-axed, irregular shape. For

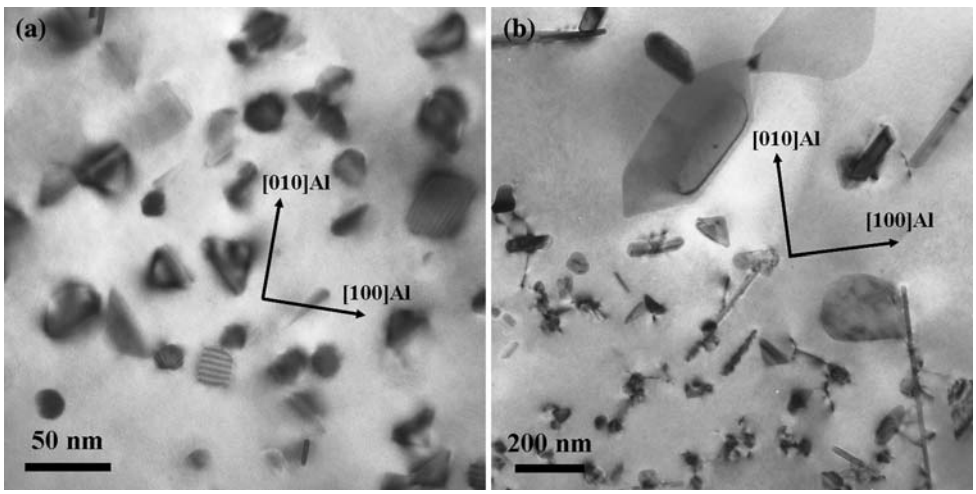

Fig. 2 ⟨001⟩Al zone axis. Bright field images of conditions 17 h_175 °C (**a**) and 3 h_260 °C (**b**) show large numbers of Si-crystals precipitated from the solid solution, having inhomogeneous distribution. Precipitate size increases with decreasing particle density. The particles have different shapes, the most common being either pyramid or lath/plate type. Note the different magnifications

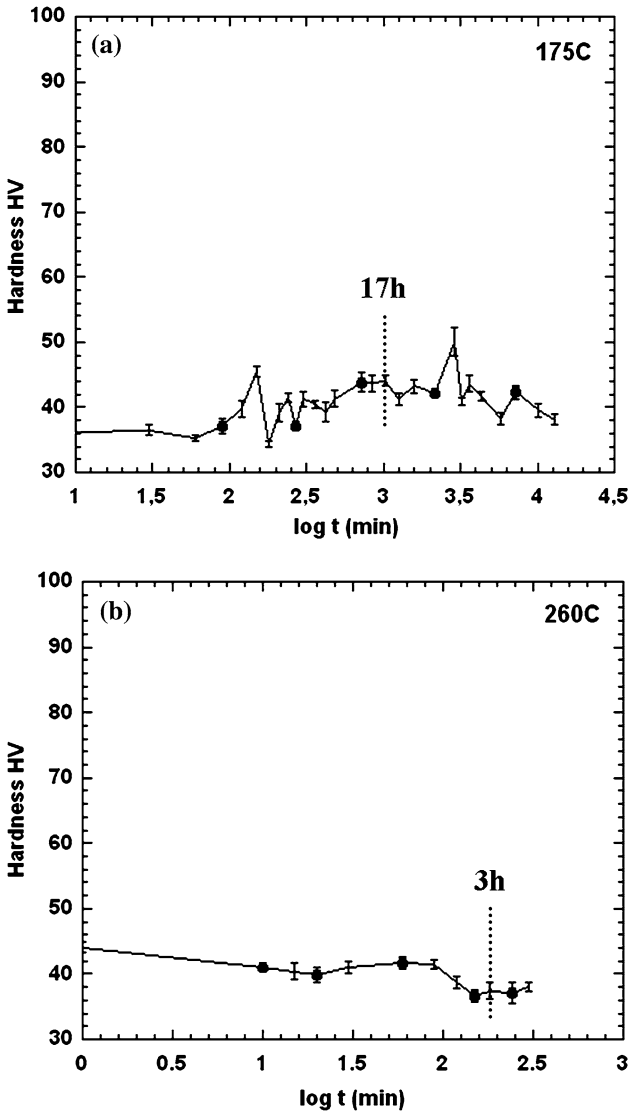

Fig. 3 Hardness curves for isothermal heat treatments at (**a**) 175 °C and (**b**) 260 °C show low material strength. The ageing time chosen for the samples investigated by TEM is indicated

the current heat-treatments, the two first shapes are the most common and appear to be related to two main orientation relationships between the fcc Al matrix and the diamond cubic Si precipitates. In the following, these orientations will be named O1 and O2:

Pyramid precipitates—orientation relation O1

Bright field images like the ones in Fig. 2 show that many particles have a triangular shape when viewed along a ⟨100⟩Al projection. The base of the triangular projections is along a ⟨110⟩Al direction and the sides are along ⟨100⟩Al directions. We can infer from the projections that the shape is actually a triangular-based pyramid, resting on a {111}Al plane, the baselines in ⟨110⟩Al directions, and

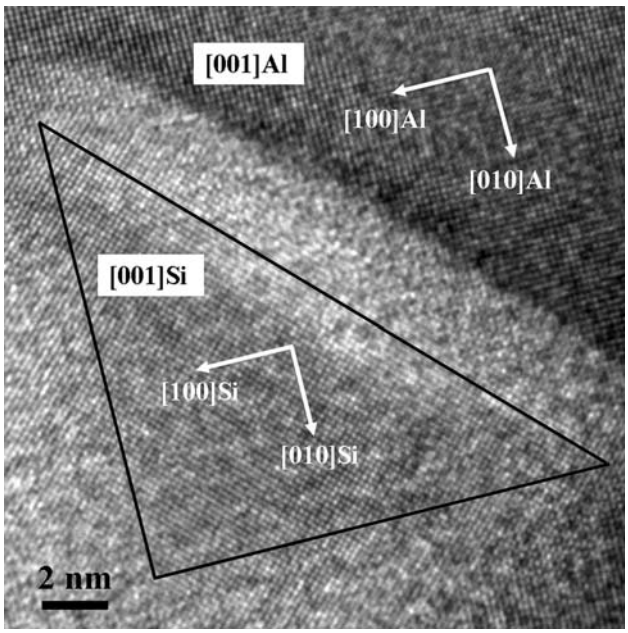

Fig. 4 High resolution image of a triangularly shaped Si-crystal from condition 17 h_175 °C having the orientation relation O1 with parallel unit cells. Some overlap with the matrix can be observed. The edges of the Si-crystal are aligned along ⟨100⟩Al and ⟨110⟩Al directions. Overlaid triangle shows how the crystal appears at smaller magnifications. The shape is a pyramid cut from a cube with corner as vertex, and base plane defined by the three nearest corners, i.e. a common {111} plane of the two cubic systems

the edges of sides in ⟨100⟩Al directions. From high resolution images of the triangular precipitates (Fig. 4) and diffraction patterns (Figs. 5 and 6) it is evident that silicon and aluminium have parallel unit cells:

$$(001)\mathrm{Al} \parallel (001)\mathrm{Si},\ [100]\mathrm{Al} \parallel [100]\mathrm{Si},\ [010]\mathrm{Al} \parallel [010]\mathrm{Si}. \quad (3)$$

This orientation will be labelled 'O1'. In Fig. 7 examples of triangular projections of the pyramids together with ⟨100⟩Al type plates, as explained below, can be found. This image suggests that most (short) streaks in ⟨110⟩ directions are not plates, but actually originate from the base of the triangular phase. One reason for appearing as short streaks is a high contrast thickness contour line commonly being parallel with the bases. Another reason is that the upper part of the pyramids is often missing, which should mean that the growth starts at the base plane, which is a specific {111}Al plane. Once attached to this plane the mismatch between the crystal structures prevents the growing Si-particle to obtain a similar match with any other {111}Al plane, and prevents a tetrahedron to form. The ratio between the two cubic cells (Si/Al) is slightly larger than 4/3. An approximate match is therefore obtained after about four (111)Al planes (9.35 Å) or three (111)Si planes (9.40 Å). Since the pyramid is not mirrored across the base

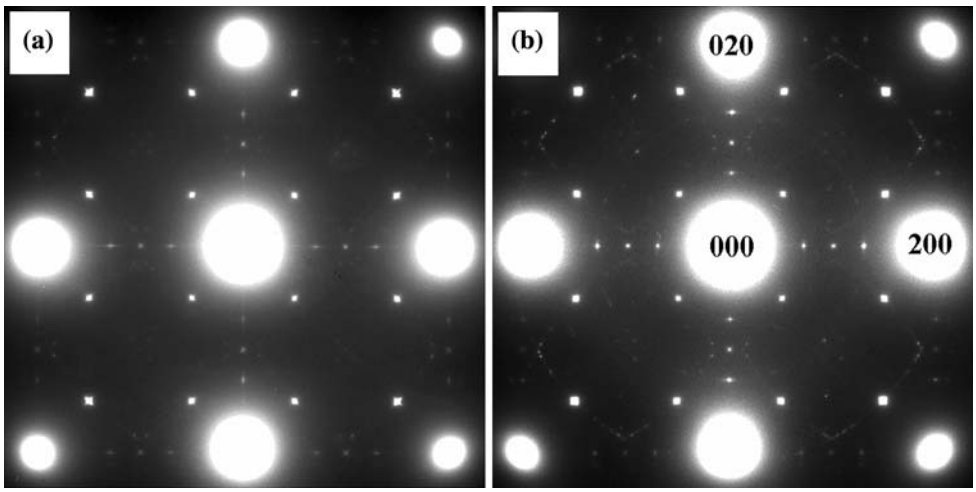

Fig. 5 SAD patterns from conditions (**a**) 17 h_175 °C and (**b**) 3 h_260 °C. In (**b**) the Al indices are shown. Orientation relations O1 and O2 can explain most of the spots. The stronger and less streaky spots in (**b**) are caused by larger particles. See Fig. 6 and text for more details

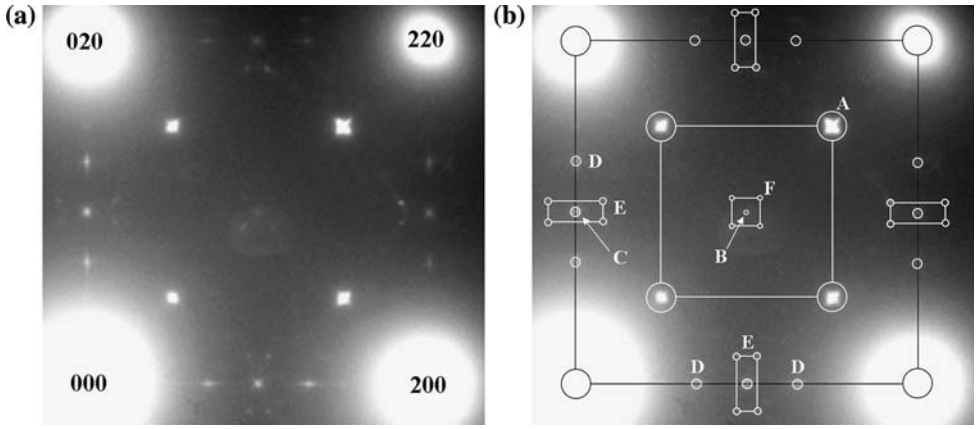

Fig. 6 Excerpt from Fig. 5a, upper right quadrant of the ⟨001⟩Al zone. The right hand side image is an overlay emphasizing sets of equivalent spots by squares or rectangles. Only the clearest are labelled. The spots that form square A are of 220Si type (indicated corner), and multiple diffractions between 220Si and 200Al, 220Al beams. These spots come from Si-crystals in orientation O1. The same orientation produces the weak spot B generated by the diffractions between 440Si and Al, and the spots C that result from diffractions between 400Si spots and Al. Spots D originate from orientation O2 when viewed along both [110]Si and [1$\bar{1}$2]Si (see Fig. 8). They are the result of interactions between 111Si type spots and Al. Spots E originate from orientation O2 as well, but when viewed along [1$\bar{1}$ $\bar{1}$] Si in Fig. 8. They are the result of interactions between 202Si type spots and Al. Spots F result from interactions between 111Si spots and Al, but originating from other orientations than O1 and O2

plane, the growth conditions on the two sides of the starting plane differ. As indicated above, the pyramidal shape is consistent with the tetrahedral particles in Al–Ge alloys [5, 7, 15], but deviates from the perfect shape because it is related to one particular {111} Al plane.

Plates/lath-shaped precipitates—orientation relation O2

As was also the case for Al–Ge alloys [5], the TEM images in Figs. 2 and 7 show that in ⟨001⟩Al projections some precipitates are rod-like and extend along ⟨100⟩Al and ⟨110⟩Al type directions. When tilting the specimen, it can usually be verified that these particles are instead plates or short laths viewed edge-on. In Figs. 8 and 9a (lower particle) smaller such particles are shown. From these figures it can be inferred that a main surface is a {111}Si plane parallel with a {010}Al plane. For the chosen reference system it can be noticed that in these particles the Al- and Si-crystals have the common orientation relationship given by Eqs. 1 and 2. In the following, this orientation will be labelled 'O2'.

With the specific orientations as indicated in Fig. 8, important habit planes have normal vectors [1$\bar{1}$ $\bar{1}$]Si || [010]Al, [1$\bar{1}$1]Si || [310]Al, [001]Si || [3$\bar{2}$0] Al and [$\bar{1}$1 0]Si || [$\bar{2}$ $\bar{3}$ 0] Al. Using the matrix in Eq. 2 the direction of the Si-vectors can be referred to the Al coordinate system, and the angular deviation relative to rational directions checked. The vectors in some of these pairs are only approximately

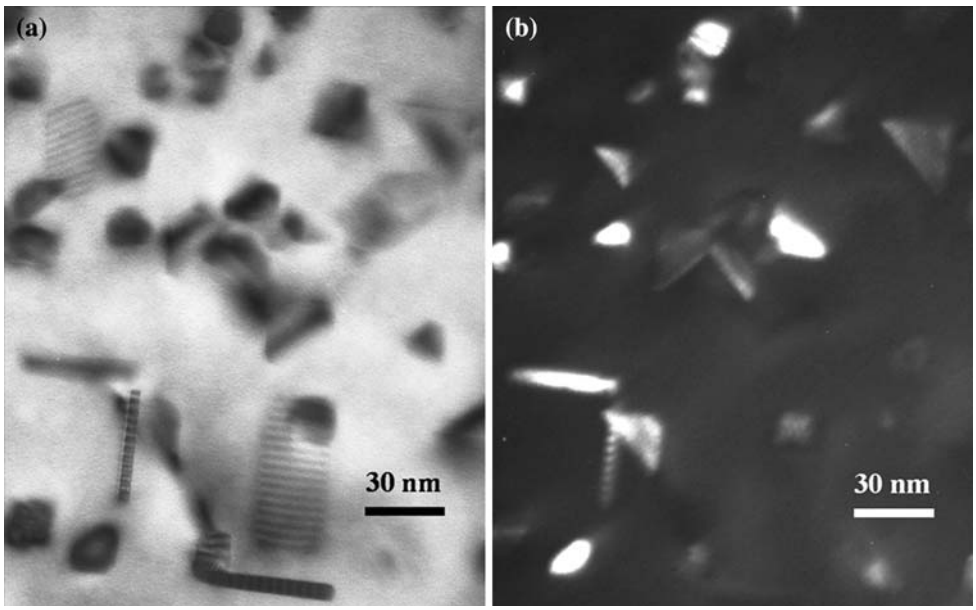

Fig. 7 (**a**) Bright field image from condition 17 h_175 °C. (**b**) Dark field image from the same area as in (**a**), where only one of the orientation O1 spots was used. From such images it could be inferred that about 60% of the total Si-crystals have orientation O1 and 40% O2

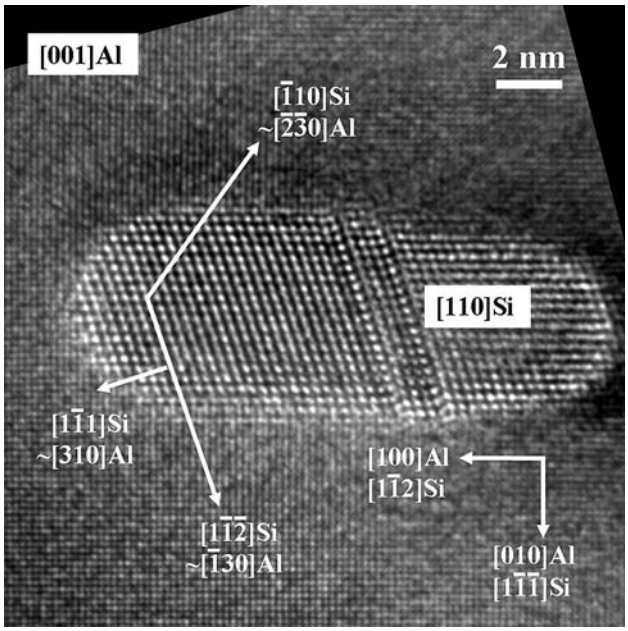

Fig. 8 High resolution image of a Si-crystal in condition 17 h_175 °C illustrates the O2 orientation relation: (001)Al || (110)Si, [1$\bar{1}$ $\bar{1}$]Si || [010]Al. The crystal has interfaces along ⟨100⟩Al, ⟨130⟩Al and ⟨230⟩Al directions. Stacking faults on (1$\bar{1}$1)Si run across the particle

parallel: The difference in direction of the pair ([1$\bar{1}$1]Si, [310]Al)is 1.04°. For the two pairs ([[001]Si, 3$\bar{2}$0] Al), ([$\bar{1}$10]Si, [$\bar{2}$ $\bar{3}$0]Al) the direction difference is 1.57°.

For relation O2 the ⟨123⟩Si directions appear to be important. The [2$\bar{1}$3], [1$\bar{3}$2] and [$\bar{3}$ $\bar{2}$ $\bar{1}$] vectors in the ([1$\bar{1}$ $\bar{1}$]) plane are 120° apart. They are 0.42°, 4.11° and 0.67° off the Al matrix vectors [501], [$\bar{1}$01] and [$\bar{1}$0$\bar{3}$], respectively. There is a special match in periodicity along [2$\bar{1}$3] Si and [501]Al, which shows up as a coherent unit-cell edge (10.4 Å) in several of the important precipitate phases in the Al–Mg–Si–(Cu) alloys [4]. The relation is $a^{Si}|[2\bar{1}3]|/2 \sim a^{Al}|[501]|/2$ the length of the vectors being 10.16 Å and 10.33 Å, respectively (1.6% difference). The basic periodicities are half these numbers, i.e. $7d^{Si}_{4\bar{2}6} \sim d^{Al}_{10,0,2}$. Relations between Si and Al can also be found for the other ⟨123⟩ directions, $2d^{Si}_{26\bar{4}} \sim d^{Al}_{20\bar{2}}$ (1.3% difference), and the less obvious $7d^{Si}_{6\bar{4}2} \sim 8d^{Al}_{20\bar{6}}$ (0.8% difference). There is a worse match in periods along the common coordinate axes: $2d^{Si}_{1\bar{1}\,\bar{1}} \sim 3d^{Al}_{020}$ (3.1%), $2d^{Si}_{2\bar{2}4} \sim d^{Al}_{200}$ (9.0%), and $d^{Si}_{220} \sim d^{Al}_{002}$ (5.2%).

We can conclude that the orientation O2 is essentially an alignment of the (010)Al plane with (1$\bar{1}$ $\bar{1}$) Si: a stack of three layers of (020)Al planes yields about 2 layers of (1$\bar{1}$ $\bar{1}$) Si. Within these planes, matches in periodicity along several of the directions can be found between the two crystals. Among these, the ⟨123⟩ directions in Si appear to be most important.

A previously reported orientation relation (O3)

A third orientation with a small rotation difference relative to O2 has been reported to be common in an Al-1.0 wt% Mg_2Si-0.4 wt% Si alloy heat-treated 100 min at 350 °C [18]. A similarly oriented plate has been found in the Al–Ge system [15]. Using the same reference system as for orientation O2, this third orientation (labelled O3) can be described as

$$(010)\text{Al} \,||(1\bar{1}\,\bar{1})\ \text{Si},\ [105]\text{Al} \,||\, [110]\text{Si},\ [50\bar{1}]\text{Al} \,||\, [1\bar{1}2]\text{Si} \quad (4)$$

Relative to O2 the O3 orientation relation can be viewed as a small rotation of the (1$\bar{1}$ $\bar{1}$) Si plane on the parallel (010)Al plane. As a result, the [110]Si direction of the plane

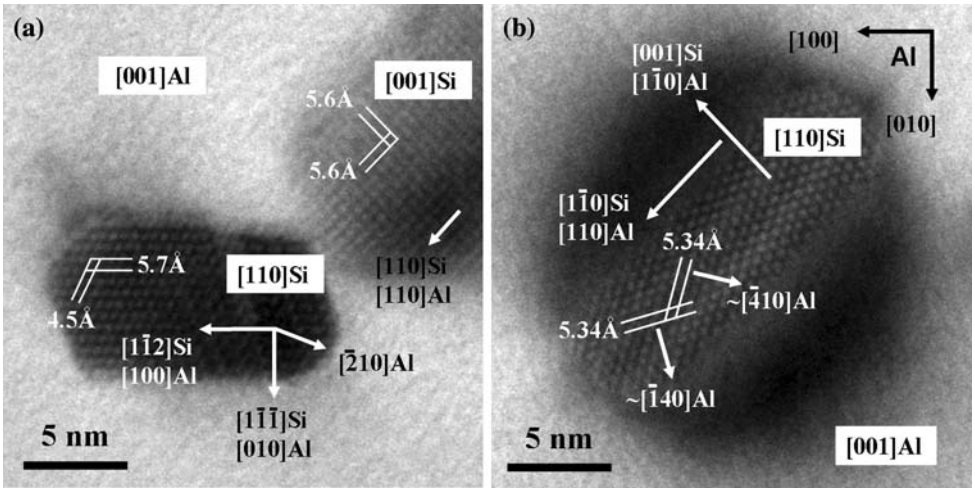

Fig. 9 Low resolution bright field images of Si-particles in a ⟨001⟩Al zone from condition 17 h_175 °C. Periodic variations are the result of Moiré fringes from overlapping Si/Al lattices generated by low index reflections. Moiré periods are indicated in the images. (**a**) Particles with the main orientation relations O1 (up-right) and O2 (lower). (**b**) Rare orientation of Si- particle: [110]Si || [001]Al, [1$\bar{1}$0]Si || [110]Al and [001]Si || [1$\bar{1}$0]Al.This is similar to the lower right variant in Fig. 10

is rotated from [001]Al to [105]Al an angle 11.3°. When viewed along (1$\bar{1}$ $\bar{1}$) Si || (010)Al the precipitates are plates shaped as equilateral triangles with sides along ⟨110⟩Si directions. They are near the following Al-directions: [110]Si||[105]Al, [101]Si||[301]Al and [0$\bar{1}$1] Si || [70$\bar{6}$]Al. In this case the [100]Al and [001]Al vectors will be near [2$\bar{1}$3] Si and [45$\bar{1}$] Si and the orientation relation may be given by the matrix:

$$R_{03} = \frac{1}{\sqrt{42}} \begin{pmatrix} 2\sqrt{3} & -\sqrt{3} & 3\sqrt{3} \\ \sqrt{14} & -\sqrt{14} & -\sqrt{14} \\ 4 & 5 & -1 \end{pmatrix}, \qquad (5)$$

which transforms coordinates of Si-vectors to the Al system. A good periodic match in directions within the parallel planes (010)Al ||(1$\bar{1}$ $\bar{1}$) Si occurs between [101]Si and [301]Al. Here $d^{Si}_{202} \sim 3d^{Al}_{602} = 1.92$ Å (0.06% difference). Also along [2$\bar{1}$3] Si ‖ [100]Al a periodic match exists. We can see this via lattice plane distances, as $14d^{Si}_{4\bar{2}6} \sim 5d^{Al}_{200} = 10.13$ Å (0.33%). In terms of the real vectors $a^{Si}|[2\bar{1}3]| = 20.32\,\text{Å} \sim a^{Al}|[500]| = 20.25$ Å. The other ⟨123⟩ directions do not seem to be important for this orientation relation. As for orientation relation O2, the stacking of the (1$\bar{1}$ $\bar{1}$) Si planes parallel with (010) Al results in a periodic match $2d^{Si}_{1\bar{1}\,\bar{1}} \sim 3d^{Al}_{020}$ (3.1%). The other main directions (Eq. 4) have similar or worse periodic matches.

To sum up, O2 and O3 orientations are essentially an alignment of the (010)Al plane with (1$\bar{1}$ $\bar{1}$) Si. In orientation O3 the [2$\bar{1}$3]Si and [101]Si directions that lay in the (1$\bar{1}$ $\bar{1}$) Si plane match best the aluminium periodicities along [100]Al and [301]Al, respectively. In O2 the [2$\bar{1}$3] Si direction also gives a good match with Al, together with other ⟨123⟩Si type directions in the (1$\bar{1}$ $\bar{1}$) Si plane.

Other shapes and less common orientation relations

A few particles were found to have a more equi-axed shape. An interesting example with pentagonal twinning is given in Fig. 10. As for the orientation relation O2, it has parallel directions ⟨110⟩Si || ⟨001⟩Al. Along the ⟨001⟩Al zone, the five variants in the Si-particle are mutually rotated around a common ⟨110⟩Si axis. We see that none of the variants have O2 relationships. It is likely that a small fraction of Si-crystals taking one or more of these variant's orientations can exist in the matrix. One such particle was found in the experiments: the particle in Fig. 9b is an example of the lower right variant of Fig. 10. The findings are entirely analogous to twinning studied in the Al–Ge

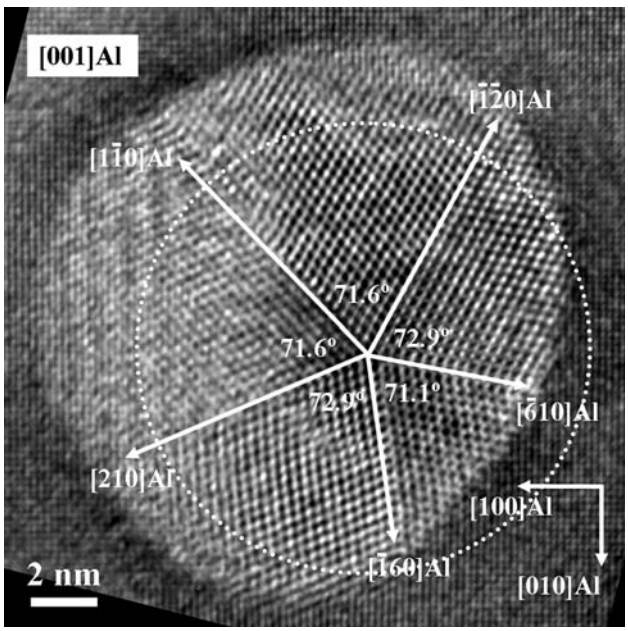

Fig. 10 Equi-axed particle: Pentagonal twins in a ⟨110⟩ Si zone parallel with ⟨001⟩Al. The directions indicated by arrows are in the Al coordinate system and correspond to ⟨112⟩Si type directions along {111}Si planes. The indicated directions in Al were estimated, whereby the angles have been calculated. The lower right variant with two {111}Si planes nearly parallel with {610}Al planes has the same orientation as the particle in Fig. 9b

system [5, 7], where all orientation relations could be explained by twinning from three orientations [5].

Moiré in the Si-particles

Many small Si-crystals are partly or completely embedded in the Al matrix. At intermediate magnifications Moiré fringes are caused by the overlapping Al and Si lattices, making the particles difficult to study. The Moiré period is related to a pair of reciprocal lattice vectors corresponding to strong, low index reflections, one from each crystal. If $\mathbf{g}_1$ and $\mathbf{g}_2$ are the reciprocal vectors from the two lattices, then $\delta\mathbf{g} = \mathbf{g}_1 - \mathbf{g}_2$ gives the direction normal to the Moiré fringes [19] that have the period $d = |\delta\mathbf{g}|^{-1}$. For an angle β between $\mathbf{g}_1$ and $\mathbf{g}_2$ vectors this periodicity can be expressed as:

$$d = \frac{d_1 d_2}{\sqrt{d_1^2 + d_2^2 - 2d_1 d_2 \cos\beta}}, \tag{6}$$

where $d_1 = |\mathbf{g}_1|^{-1}$, $d_2 = |\mathbf{g}_2|^{-1}$ are the inter-planar distances of the atomic planes indicated by $\mathbf{g}_1$ and $\mathbf{g}_2$, respectively.

Figure 9 shows bright field images taken with an objective aperture excluding spatial frequencies less than approximately 4 Å. Only Moiré periods exceeding this number will then be visible in the images. Such images were used to verify the orientations of many of the particles.

Moiré and orientation relation O1

The low magnification images frequently show a square symmetry, like the upper crystal in Fig. 9a. Here, a Moiré period of 5.6 Å (±0.1 Å) is measured in two ⟨110⟩Al directions. Along [110]Al this can be interpreted as interaction of the pair $\mathbf{g}^{\mathrm{Al}}_{220}$ and $\mathbf{g}^{\mathrm{Si}}_{220}$. A similar pair interacts for the other $[1\bar{1}0]$Al direction. The inter-planar distances are $d^{\mathrm{Al}}_{220} = 1.43$ Å and $d^{\mathrm{Si}}_{220} = 1.92$ Å. Because the directions are parallel ($\beta = 0$) the Moiré formula (6) gives the measured spacing $|\delta\mathbf{g}|^{-1} = 5.6$ Å.

Moiré and orientation relation O2

A common sight in the ⟨100⟩Al zone projection is the lower particle in Fig. 9a. It is clearly similar to the particle shown in high resolution in Fig. 8, corresponding to orientation O2. The indicated Moiré periods can be explained the following way: Along [010]Al, the measured fringe period is 5.7 Å (±0.1 Å). Because the [010]Al direction is parallel to $[1\bar{1}\,\bar{1}]$ Si($\beta = 0$), this Moiré is produced by an interaction of $\mathbf{g}^{\mathrm{Si}}_{1\bar{1}\,\bar{1}}$ and $\mathbf{g}^{\mathrm{Al}}_{220}$ with lattice spacing 3.135 Å and 2.025 Å, respectively, yielding a period 5.7 Å. Another main fringe period is along the $[2\bar{1}0]$ Al direction, estimated to be 4.5 Å (±0.1 Å). We find that $\mathbf{g}^{\mathrm{Si}}_{1\bar{1}1}$ and $\mathbf{g}^{\mathrm{Al}}_{200}$ can explain the period and direction. These vectors have angular separation $\beta = 19.45°$ and the difference vector will be directed approximately along $[2\bar{1}0]$Al.

Moiré from particles having other orientation relations

One Si-crystal was found with a special orientation relation. It is shown in Fig. 9b. This particular crystal has an apparent three-fold symmetry, which would indicate a ⟨111⟩ projection. It is instead viewed along [110]Si || [001]Al., but with a different orientation relation than O2:

$$(110)\mathrm{Si}\,||\,(001)\mathrm{Al},\ [1\bar{1}0]\mathrm{Si}\,||\,[110]\mathrm{Al}\ \text{and}\ [001]\mathrm{Si}\,||\,[1\bar{1}0]\mathrm{Al}. \tag{7}$$

This means that $[1\bar{1}\,\bar{1}]$Si and $[\bar{1}1\bar{1}]$Si fall approximately along [160]Al and $[\bar{6}\,\bar{1}0]$Al. The crystal is therefore oriented like the lower right twin in the pentagonal twinned crystal in Fig. 10. The hexagonal pattern in Fig. 9b is formed by two sets of Moiré fringes with 5.34 Å periodicity, each originating from the interaction of similar planes. One Moiré set arises from the interaction of vectors $\mathbf{g}^{Si}_{1\bar{1}1}$ and $\mathbf{g}^{\mathrm{Al}}_{200}$ that have angular separation $\beta = 9.74°$. These fringes are approximately oriented along $[\bar{4}10]$Al. The other set is generated by the interaction of vectors $\mathbf{g}^{Si}_{1\bar{1}\,\bar{1}}$ and $\mathbf{g}^{\mathrm{Al}}_{020}$ with the same angular separation as before. These fringes are approximately oriented along $[\bar{1}40]$Al.

Selected area diffraction and fraction of particles with O1 and O2

Figure 5 gives examples of selected area diffraction (SAD) patterns from areas including many particles of the two heat-treatments (c.f. Fig. 2). The two investigated conditions contain the same set of spots. The higher temperature (b) is seen to reshape many spots from a streaky to a pointed appearance, and improves visibility. This suggests that thinner plates are less common in the higher temperature heat-treatment. In Fig. 6 the upper right quadrant of Fig. 5a is magnified and equivalent spots are pointed out, with an explanation of their origin. Most of the spots originate from double diffracted Si spots on 200Al, 220Al type spots. Diffracted spots A, B and C from particles with orientation relation O1 are bright because all the 24 possible orientations a Si-particle can have along an ⟨001⟩Al zone are identical along the viewing direction (neglecting shape effects), and the scattered intensity is distributed on the same few spots. The spots D and E (the rectangle E corners) that originate from orientation O2 have lower intensity. The reason is low symmetry of the combined system particle/matrix in this orientation, i.e. the intensity

is distributed among a higher number of reflections. The presence of weak spots F confirms the high resolution (Fig. 10) and Moiré pattern (Fig. 9b) observations that a low amount of other Si orientations than O1 and O2 must exist in the Al matrix. Although the origin of spots F cannot be unambiguously given, they can be explained as being double diffracted 111Si spots from Si oriented as the two upper left crystals in Fig. 10 (sharing a common $[1\bar{1}2]$Si || $[1\bar{1}0]$Al direction).

In Fig. 6 the most important reflections have been addressed, and the remaining visible spots are few with quite low intensity. The better resolution in Fig. 5b, due to the larger particles in this condition, gives the possibility of further analysis. We confirmed that most of the spots not annotated in Figs. 5 and 6 (not shown because of the low contrast) are generated by Si-crystals of orientation O2. The SAD analysis therefore confirms the observation from high resolution and Moiré images that the majority of Si-crystals nucleated in the Al matrix belong to orientations O1 and O2.

By knowing the positions in the SAD patterns of the spots from both O1 and O2 orientations, standard dark field (DF) imaging can be used to estimate the fraction of Si-crystals in the two orientations. Reflections from the orientation O1 are ideal to use for this purpose. Thanks to the high combined symmetry, every particle in this orientation will contribute to one of the spots A (Fig. 6). The corner furthest from the origin was used, which is a 220Si reflection. The relative number fraction may be found under the assumption that most of the non-exited crystals belong to orientation O2. As an example, Fig. 7 shows the bright field (BF) and the corresponding DF image of an area. For similar images in condition 17 h_175 °C, of a total of 116 Si-particles 73 (63%) were found with orientation O1.

Relative fraction of precipitates from HREM images

One disadvantage of using the DF method to determine particle fractions is the close proximity of diffracted spots from both O1 and O2 orientations, and possible overlap between the orientations. The many more possibilities of particle orientations in O2, however, reduce the errors. An additional method was employed to find the relative fractions of the two main orientation relations, using a smaller set of particles in the condition 17 h_175 °C. Here 26 precipitates were analysed in high resolution TEM images, where the crystallographic orientation could be accurately determined, see Figs. 4 and 8. Among those precipitates, 15 (58%) had orientation O1. We conclude therefore that the particles divide roughly 60:40 on the two orientation relations O1:O2, with a small fraction on other rare orientations. This result applies strictly for condition 17 h_175 °C. However, it is seen that the SAD patterns and orientations in the condition 3 h_260 °C are similar, and we expect the same number to apply also for this condition.

Conclusions

An Al–1.3at%Si alloy has been investigated by transmission electron microscopy. Hardness was measured for isothermal heat-treatments at 175 °C and 260 °C. Conditions investigated by TEM were 17 h_175 °C and 3 h_260 °C. Both contained a high density of small Si-crystals, the finest corresponding to 175 °C. The shapes of the particles were either pyramidal or a lath/plate type. The Si-crystals have been found to take two main crystallographic orientations with respect to the Al matrix:

(i) Orientation O1: (001)Al || (001)Si, [100]Al || [100]Si, [010]Al || [010]Si. Here the Al and Si have aligned cubic cells. The particles are commonly shaped like pyramids, resting on a common {111} plane, most likely the (starting) growth plane. Approximately 60% of the analysed Si precipitates from the 175 °C condition was found in orientation O1.

(ii) Orientation O2: (110)Si||(001)Al, $1\bar{1}\ \bar{1}$Si || [010]Al, Si || [100]Al. The particles are usually plate- or lath-shaped with the main face being a (111)Si plane parallel with a (100) Al plane, in which the common directions ⟨123⟩Si align with ⟨510⟩Al because of matching periodicities. This is also the orientation that can be linked to all Mg–Si containing precipitates in the important Al–Mg–Si–(Cu) systems.

Although a high number of Si-particles were formed during the isothermal heat treatments, the material hardness was low. It is about three times lower than what is achieved in similarly heat-treated Al–Mg–Si alloys, for example with half the Si substituted by Mg. Only non-coherent interfaces were observed between the Si-particles and Al matrix, which is probably the major reason for such difference in hardness.

Acknowledgements This work was financially supported by *The Research Council of Norway* via two projects: 177600/V30 "Fundamental investigations of solute clustering and nucleation of precipitation" and project 176816/I40 "Nucleation control for optimised properties", which is also supported by Hydro Al and Steertec Raufoss AS.

References

1. Marioara CD, Andersen SJ, Zandbergen HW, Holmestad R (2005) Metall Mater Trans 36A:691
2. Edwards GA, Stiller K, Dunlop GL, Couper MJ (1998) Acta Mater 46:3893
3. Andersen SJ, Marioara CD, Vissers R, Frøseth A, Zandbergen HW (2007) Mat Sci Eng A 444:157

4. Marioara CD, Andersen SJ, Stene TN, Hasting H, Walmsley J, Van Helvoort ATJ, Holmestad R (2007) Phil Mag 87:3385
5. Douin J, Dahmen U, Westmacott KH (1991) Phil Mag B 63:867
6. Hinderberger S, Xiao SQ, Westmacott KH, Dahmen U (1996) Z Mettalkd 87:161
7. Xiao SQ, Hinderberger S, Westmacott KH, Dahmen U (1996) Phil Mag A 73:1261
8. Hinderberger S, Dahmen U, Xiao SQ, Westmacott KH (2000) Z Mettalkd 91:215
9. Mitlin D, Radmilovic V, Dahmen U, Morris JW Jr (2001) Metall Mater Trans 32A:197
10. Mitlin D, Dahmen U, Radmilovic V, Morris JW Jr (2001) Mat Sci Eng A 301:231
11. Radmilovic V, Dahmen U, Dracup B, Miller MK, Mitlin D, Morris JW (2002) Mater Sci For 396–402:905
12. Mitlin D, Radmilovic V, Morris JW Jr, Dahmen U (2003) Metall Mater Trans 34A:735
13. Radmilovic V, Mitlin D, Tolley AJ, Dahmen U, Morris JW Jr (2003) Metall Mater Trans 34A:543
14. Radmilovic V, Miller MK, Mitlin D, Dahmen U (2006) Scr Mater 54:1973
15. Kaneko K, Inoke K, Sato K, Kitawaki K, Higashida H, Arslan I, Midgley PA (2008) Ultramicr 108:210
16. Marioara CD, Nordmark H, Andersen SJ, Holmestad R (2006) J Mater Sci 41:471
17. Hornbogen E, Mukhopadhyay AK, Starke EA Jr (1992) Z Metallkd 83:577
18. Matsuda K, Tada S, Ikeno S (1994) J Jpn Inst Metals 58:252
19. Williams DB, Carter CB (1996) Transmission Electron Microscopy. Plenum Press, New York, p 445